ADVANCED FUNCTIONAL MATERIALS
www.afm-journal.de

Amino *N*-Oxide Functionalized Conjugated Polymers and their Amino-Functionalized Precursors: New Cathode Interlayers for High-Performance Optoelectronic Devices

Xing Guan, Kai Zhang, Fei Huang, Guillermo C. Bazan,* and Yong Cao*

A series of amino *N*-oxide functionalized polyfluorene homopolymers and copolymers (PNOs) are synthesized by oxidizing their amino functionalized precursor polymers (PNs) with hydrogen peroxide. Excellent solubility in polar solvents and good electron injection from high work-function metals make PNOs good candidates for interfacial modification of solution processed multilayer polymer light-emitting diodes (PLEDs) and polymer solar cells (PSCs). Both PNOs and PNs are used as cathode interlayers in PLEDs and PSCs. It is found that the resulting devices show much better performance than devices based on a bare Al cathode. The effect of side chain and main chain variations on the device performance is investigated. PNOs/Al cathode devices exhibit better performance than PNs/Al cathode devices. Moreover, devices incorporating polymers with para-linkage of pyridinyl moieties exhibit better performance than those using polymers with meta-linked counterparts. With a poly[(2,7-(9,9-bis(6-(*N*,*N*-diethylamino)-hexyl *N*-oxide)fluorene))-alt-(2,5-pyridinyl)] (PF6NO25Py) cathode interlayer, the resulting device exhibits a luminance efficiency of 16.9 cd A^{-1} and a power conversion efficiency of 6.9% for PLEDs and PSCs, respectively. These results indicate that PNOs are promising new cathode interlayers for modifying a range of optoelectronic devices.

1. Introduction

Conjugated-polymer-based organic electronic devices, such as polymer light-emitting diodes (PLEDs)[1] and polymer solar cells (PSCs),[2] have attracted considerable attention recently due to their unique characteristics, such as low cost, light weight, and possible flexibility and large-area coverage. Both PLEDs and PSCs usually adopt a basic architecture composed of a thin layer of organic semiconducting material sandwiched between two electrodes. It is therefore important to control the properties of the organic/electrode interface to maximize performance.[3] For PLEDs, interface layers with good hole/electron transporting/injection properties are required to optimize charge injection, transport, and recombination.[3b,4,5] Interface modification is also desired to maximize charge extraction in high performance PSCs.[3,5] Low work-function cathodes (such as Ba and Ca) can be used in both types of devices to achieve high efficiency at the expense of sensitivity toward moisture and oxygen.[6] Air-stable high work-function metals (such as Al, Ag, and Au) are therefore desired to improve stability. In order to minimize the energy barrier between the active layer and high work-function metals, it is necessary to introduce an interfacial layer between the active layer and the metal electrode, such as LiF,[7] $CsCO_3$,[8] TiO_x,[9] or organic surfactants.[10]

Water/alcohol soluble conjugated polymers (WSCPs) have been recently used in PLEDs[11] and PSCs[12] as cathode interlayers.[5f,13] Their solubility in high polar solvents allows the fabrication of multilayer devices through solution-processing. Based on these unique characteristics, high-efficiency all printable PLEDs have been realized.[14] WSCPs interlayers can also enhance the short-circuit current density (J_{sc}), open-circuit voltage (V_{oc}), and fill factor (*FF*), thus improve the power conversion efficiency (*PCE*) of PSCs.[12] Conjugated polyelectrolytes (CPEs), a typical kind of WSCPs, have been extensively examined. However, mobile counter ions may migrate into the emission layer (EML) and induce luminescence quenching and affect the long-term stability of devices.[15] Moreover, the response times of the devices can be influenced by the nature of their counter ions.[11d,16] New WSCPs with highly polar but non-ionic functionalities[11g,17] are therefore desirable and are challenging to prepare due to the combination of polar pendant groups and highly hydrophobic main chains.

X. Guan, K. Zhang, Prof. F. Huang,
Prof. G. C. Bazan, Prof. Y. Cao
State Key Laboratory of Luminescent Materials and Devices
Institute of Polymer Optoelectronic Materials and Devices
South China University of Technology
Guangzhou 510640, P. R. China
E-mail: msfhuang@scut.edu.cn; bazan@chem.ucsb.edu
Prof. G. C. Bazan
Center for Polymers and Organic Solids
Department of Physics and Department of Chemistry and Biochemistry
University of California Santa Barbara
Santa Barbara, CA 93106, USA

DOI: 10.1002/adfm.201200199

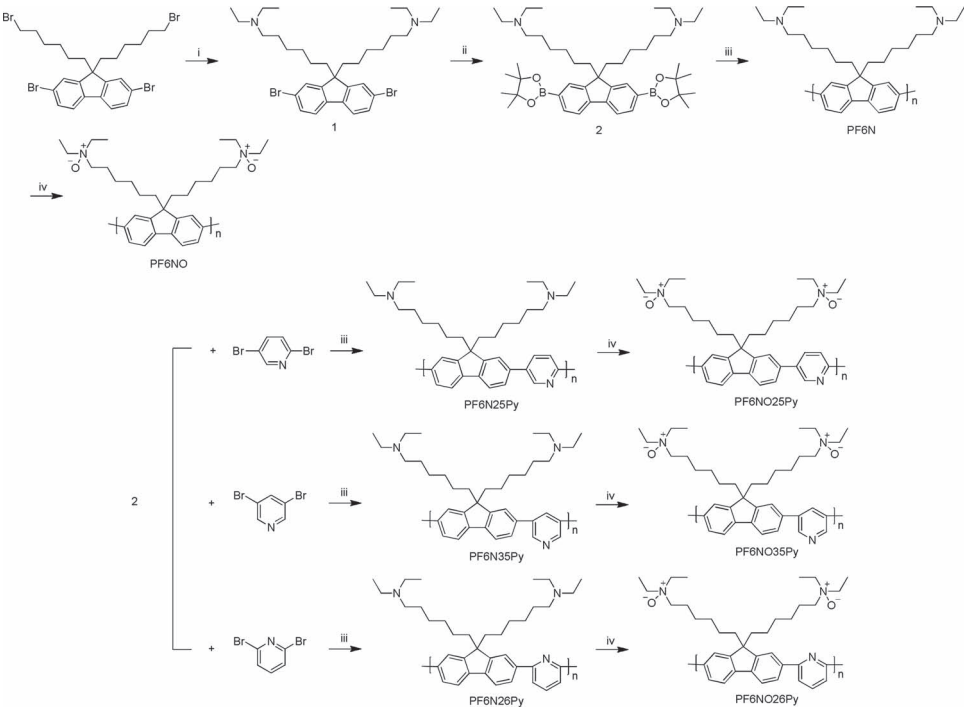

Scheme 1. Structure and synthetic route of the monomers and polymers. Reagents and conditions: i) diethylamine, DMF, reflux; ii) n-butyllithium, THF, –78 °C, then 2-isopropoxy-4,4,5,5-tetramethyl-(1,3,2)-dioxaborolane, ambient temperature; iii) $Pd(PPh_3)_4$, tetraethylammonium hydroxide 20% aq., toluene, reflux, 24 h; and iv) hydrogen peroxide 30% aq., methanol, ambient temperature, 48 h.

Amine *N*-oxides are amine-based amphoteric surfactants[18] with large dipole moments[19] and excellent solubility in polar solvents. These characteristics suggest that amino *N*-oxide functionalized WSCPs can be promising new materials for interfacial engineering. Herein, we report the development of the first class of amino *N*-oxide functionalized WSCPs and their incorporation in polymer optoelectronic devices. As shown in **Scheme 1**, four amino *N*-oxide functionalized WSCPs with different conjugated main chains, poly[9,9-bis(6-(*N*,*N*-diethylamino)-hexyl *N*-oxide)fluorene (PF6NO), poly[(2,7-(9,9-bis(6-(*N*,*N*-diethylamino)-hexyl *N*-oxide)fluorene))-*alt*-(2,5-pyridinyl)] (PF6NO25Py), poly[(2,7-(9,9-bis(6-(*N*,*N*-diethylamino)-hexyl *N*-oxide)fluorene))-*alt*-(2,6-pyridinyl)] (PF6NO26Py), poly[(2,7-(9,9-bis(6-(*N*,*N*-diethylamino)-hexyl *N*-oxide)fluorene))-*alt*-(3,5-pyridinyl)] (PF6NO35Py) and their amino functionalized precursor polymers poly[9,9-bis(6-(*N*,*N*-diethylamino)-hexyl)fluorene] (PF6N), poly[(2,7-(9,9-bis(6-(*N*,*N*-diethylamino)-hexyl)fluorene))-*alt*-(2,5-pyridinyl)] (PF6N25Py), poly[(2,7-(9,9-bis(6-(*N*,*N*-diethylamino)-hexyl) fluorene))-*alt*-(2,6-pyridinyl)] (PF6N26Py), poly[(2,7-(9,9-bis(6-(*N*,*N*-diethylamino)-hexyl)fluorene))-*alt*-(3,5-pyridinyl)] (PF6N35Py), were developed and used as cathode interlayers. The relationships between chemical structure and optoelectronic properties were also systematically investigated. It was found that the pendant amino *N*-oxide groups not only enhance the alcohol solubility of the polymers, but also improve their electron injection/extraction ability when incorporated as interlayers in organic optoelectronic devices.

2. Results and Discussion

2.1. Design, Synthesis, and Characterization

Scheme 1 shows the synthetic route for the relevant monomers and polymers. Monomer 2,7-dibromo-9,9-bis(6-(*N*,*N*-diethylamino)hexyl)fluorene (**1**) was synthesized by reacting 2,7-dibromo-9,9-bis(6-bromohexyl)fluorene[20] with excess diethylamine in *N*,*N*-dimethylformamide (DMF) under argon. The key intermediate 2,7-bis(4,4,5,5-tetramethyl-1,3,2-dioxaborolane-2-yl)-9,9-bis(6-(*N*,*N*-diethylamino)-hexyl)fluorene (**2**) was synthesized in 82% yield by reacting **1** with n-butyllithium at –78 °C under argon, followed by quenching with 2-isopropoxy-4,4,5,5-tetramethyl-1,3,2-dioxaborolane and the product was purified by recrystallization from acetone. Copolymerization of **2** with either 2,5-dibromopyridine, 3,5-dibromopyridine or 2,6-dibromopyridine was using the standard Pd-catalyzed Suzuki cross-coupling conditions afforded the precursor polymers (PNs) PF6N, PF6N25Py, PF6N35Py, and PF6N26Py (see Scheme 1) in 79–91% yields. Their chemical structures were confirmed by ^{1}H NMR spectroscopy. The number average molecular weights (M_n) estimated by gel permeation chromatography (GPC) using polystyrene standards and tetrahydrofuran (THF) as the eluent are 13 500 (with a polydispersity (*PDI*) of 1.4) for PF6N, 22 400 (*PDI* = 1.6) for PF6N25Py, 12 100 (*PDI* = 1.6) for PF6N26Py and 10 300 (*PDI* = 1.6) for PF6N35Py, respectively. The final amino *N*-oxide functionalized polymers (PNOs) PF6NO, PF6NO25Py,

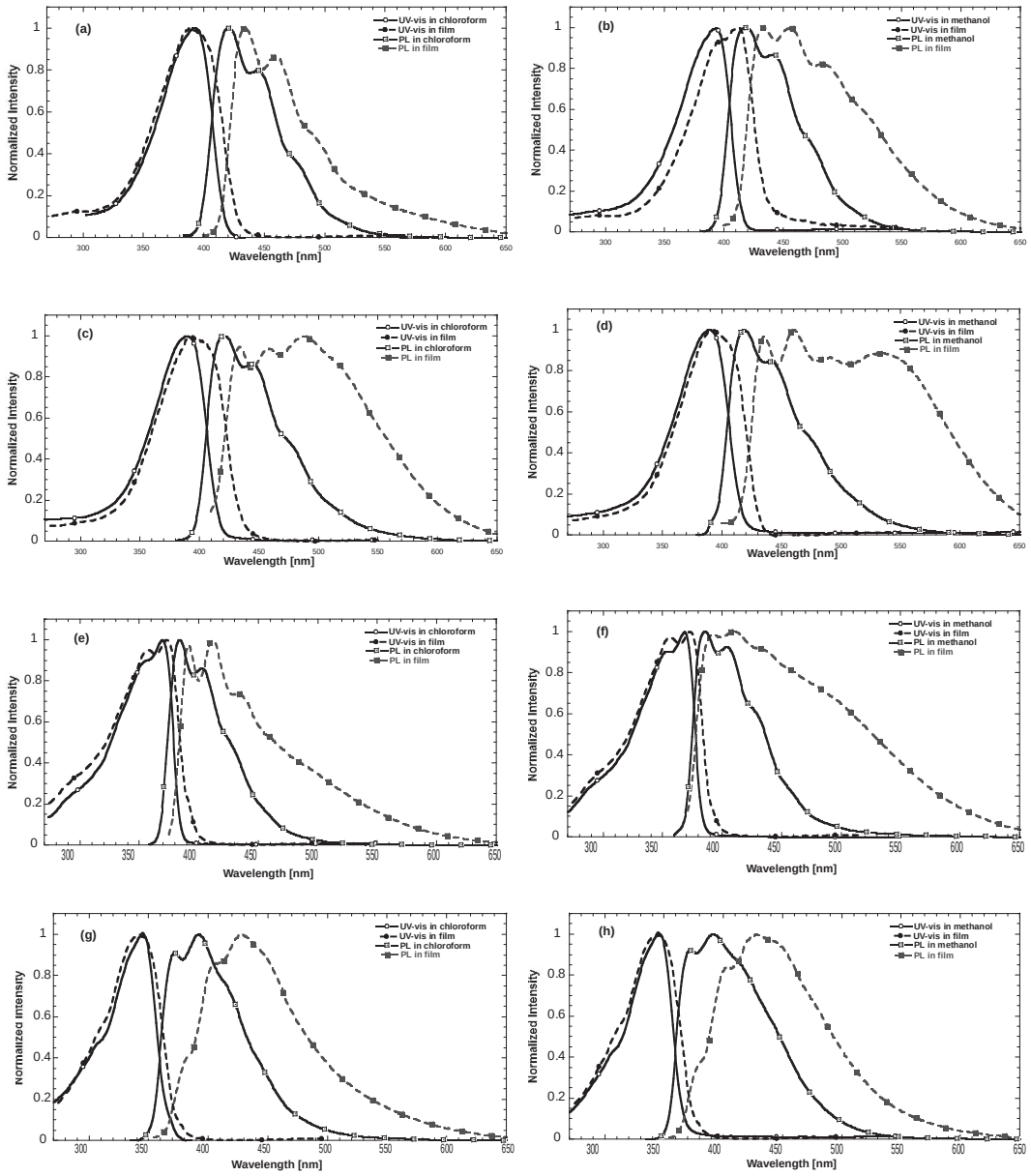

Figure 1. UV-vis absorption and PL emission spectra of polymers in solution (chloroform for PF6N, PF6N25Py, PF6N26Py, and PF6N35Py; methanol for PF6NO, PF6NO25Py, PF6NO26Py, and PF6NO35Py) and in solid-state films. a) PF6N, b) PF6NO, c) PF6N25Py, d) PF6NO25Py, e) PF6N26Py, f) PF6NO26Py, g) PF6N35Py, and h) PF6N35OPy.

PF6NO35Py, and PF6NO26Py were obtained by oxidizing the corresponding precursor polymers with excess hydrogen peroxide in methanol at room temperature for 2 days. Because of the mild oxidation conditions, only the nitrogen atoms in pendant tertiary amino groups are oxidized.

Relative to an unsubstituted phenyl unit, the presence of conjugated pyridinyl moieties in the PNO main chains is anticipated to increase the electron affinity of the material, increase resistance to oxidation and improve their electron injection ability in PLEDs.[21] Polymers with para-linkages (2,5-substitution) have more effective conjugation length than those with meta-linkages (2,6- or 3,5-substitution).[22] The amino *N*-oxide functionalized side chains endow PNOs with excellent solubility in polar solvents such as methanol, DMF, and dimethyl sulfoxide (DMSO). In contrast, their precursor polymers PNs can only dissolve in relative low polarity solvents such as toluene, THF, and chloroform. Nevertheless, PNs are soluble in methanol in the presence of trace acetic acid because of the weak interaction between the nitrogen atoms in amine or pyridine and the acetic acid.[11a,23]

2.2. Optical and Electrochemical Properties

Figure 1 shows the UV-vis absorption and photoluminescence (PL) spectra of the polymers in chloroform for PNs,

Table 1. UV-vis absorption, PL, and electrochemical properties of the polymers.

Polymer	Solution		Film				
	λ_{abs} [nm]	λ_{PL} [nm]	λ_{abs} [nm]	λ_{PL} [nm]	Optical Band Gap [eV]	HOMO [eV][c)]	LUMO [eV][d)]
PF6N	391[a)]	420[a)]	391	433	2.90	–5.49	–2.59
PF6NO	392[b)]	418[b)]	412	434	2.88	–5.50	–2.62
PF6N25Py	390[a)]	420[a)]	394	487	2.90	–5.56	–2.66
PF6NO25Py	389[b)]	419[b)]	393	460	2.87	–5.60	–2.73
PF6N26Py	369[a)]	384[a)]	373	412	3.20	–5.76	–2.54
PF6NO26Py	368[b)]	386[b)]	373	412	3.19	–5.73	–2.54
PF6N35Py	344[a)]	392[a)]	345	427	3.37	–5.67	–2.30
PF6NO35Py	345[b)]	392[b)]	346	427	3.33	–5.69	–2.36

[a)]In chloroform; [b)]In methanol; [c)]HOMO energy values were deduced from cyclic voltammetry; [d)]LUMO energy values were estimated from the π–π^* gap, together with HOMO values.

methanol for PNOs, and in the solid-state. As summarized in **Table 1**, the absorption peak of PF6N in chloroform is observed at 391 nm. The corresponding PL spectrum peaks at 420 nm with a vibronic shoulder at 445 nm. PF6N25Py shows similar absorption spectra as PF6N. While PF6N26Py and PF6N35Py exhibit an obvious blue shift in the absorption spectra as compared with that of PF6N and PF6N25Py. This could be attributed to the lesser effective π electron delocalization in the polymer main chain arising from the meta-linkage of pyridinyl moieties.[22] Similar trends were also observed in the PL spectra of PF6N25Py, PF6N26Py and PF6N35Py in chloroform. The PL spectra of PF6N25Py, PF6N26Py and PF6N35Py peak at 420, 384, and 392 nm with vibronic shoulders at 443, 404, and 371 nm, respectively. PNOs show similar absorption and emission spectra to their precursor polymers in solution; side group functionalization therefore provides negligible perturbation of the electronic properties of the backbone.

The optical properties of polymers in the film state are also summarized in Figure 1 and Table 1. Transparent and uniform films can be prepared on quartz plates by spin-casting from chloroform solutions for PNs and methanol solutions for PNOs. Compared with their absorption spectra in solution, the spectra of PF6N26Py, PF6NO26Py, PF6N35Py, and PF6NO35Py in thin films show only a slight red shift, while those of PF6N, PF6NO, PF6N25Py, and PF6NO25Py in thin film show a more pronounced red shift. This trend is probably due to the more effective conjugation in the latter polymers. All PNs and PNOs show more red-shifted emission in thin film than in solution. Noticeablely, PNOs show broader and more red-shifted emission in thin film than for PNs, which may probably be attributed to stronger interchain contacts induced by amino *N*-oxide groups.[24] Both PF6N25Py and PF6NO25Py exhibit more red-shifted and broader PL spectra in thin film compared to PF6N26Py, PF6NO26Py, PF6N35Py, and PF6NO35Py, suggesting more pronounced aggregation of polymer chains as would be expected on the basis of their more rigid backbone structures.[24] The optical bandgaps of the polymers were estimated by using their absorption onset of the films and are summarized in Table 1.

The electrochemical properties of the polymers were investigated by cyclic voltammetry (CV) in argon-saturated anhydrous solutions of 0.1 M tetrabutylammonium hexafluorophosphate (Bu_4NPF_6) in acetonitrile at a scan rate of 50 mV s^{-1} at room temperature. A platinum electrode was coated with a polymer thin film and was used as the working electrode. A Pt wire was used as the counter electrode, and Ag/Ag^+ (0.1 M of $AgNO_3$ in acetonitrile) was used as the reference electrode. The highest occupied molecular orbital (HOMO) energy levels of PF6N, PF6N25Py, PF6N26Py, and PF6N35Py were calculated to be –5.49, –5.56, –5.76, and –5.67 eV, respectively, using ferrocence value of 4.8 eV as the internal standard.[25] By introducing the electron withdraw units pyridinyl in the polyfluorenes main chain, the HOMO levels of these polymers decreased compared to that of PF6N. Polymers with meta-linkage of pyridinyl moieties had lesser conjugation length and showed lower HOMO levels. The LUMO energy levels of these polymers were calculated by using their optical band gaps and HOMO energy levels. The LUMO levels of PF6N, PF6N25Py, PF6N26Py, and PF6N35Py were –2.59, –2.66, –2.56, and –2.30 eV, respectively. PNOs showed similar HOMO and LUMO levels as their precursor polymers PNs.

2.3. Cathode Interlayer Function in PLEDs

To investigate the electron injection properties PNs and PNOs in PLEDs, a green-emitting polymer poly[2-(4-(3′,7′-dimethyloctyloxy)-phenyl)-*p*-phenylenevinylene] (P-PPV) was used as the emitting layer in PLEDs, with device configuration of indium tin oxide (ITO)/poly(3,4-ethylenedioxythiophene):poly (styrene sulfonic acid) (PEDOT:PSS)/P-PPV/Interlayer/Al. The PNs and PNOs were spin-coated from methanol/acetic acid and methanol solution onto the P-PPV layer, respectively, followed by evaporation of an 80 nm thick Al cathode. For comparison, Al, CsF/Al and Ba/Al were also used as cathodes.

Figure 2a,b show the current density (*J*) and luminance (*L*) versus voltage (*V*) characteristics of different devices. Figure 2c,d show the luminance efficiency (*LE*) versus *J* characteristics of different devices. Figure 2e shows the electroluminescence (EL) spectra of the PLEDs. **Table 2** summarizes device performance at J = 35 mA cm^{-2}. Figure 2e shows that all devices give similar EL spectra; this observation indicates that their exciton

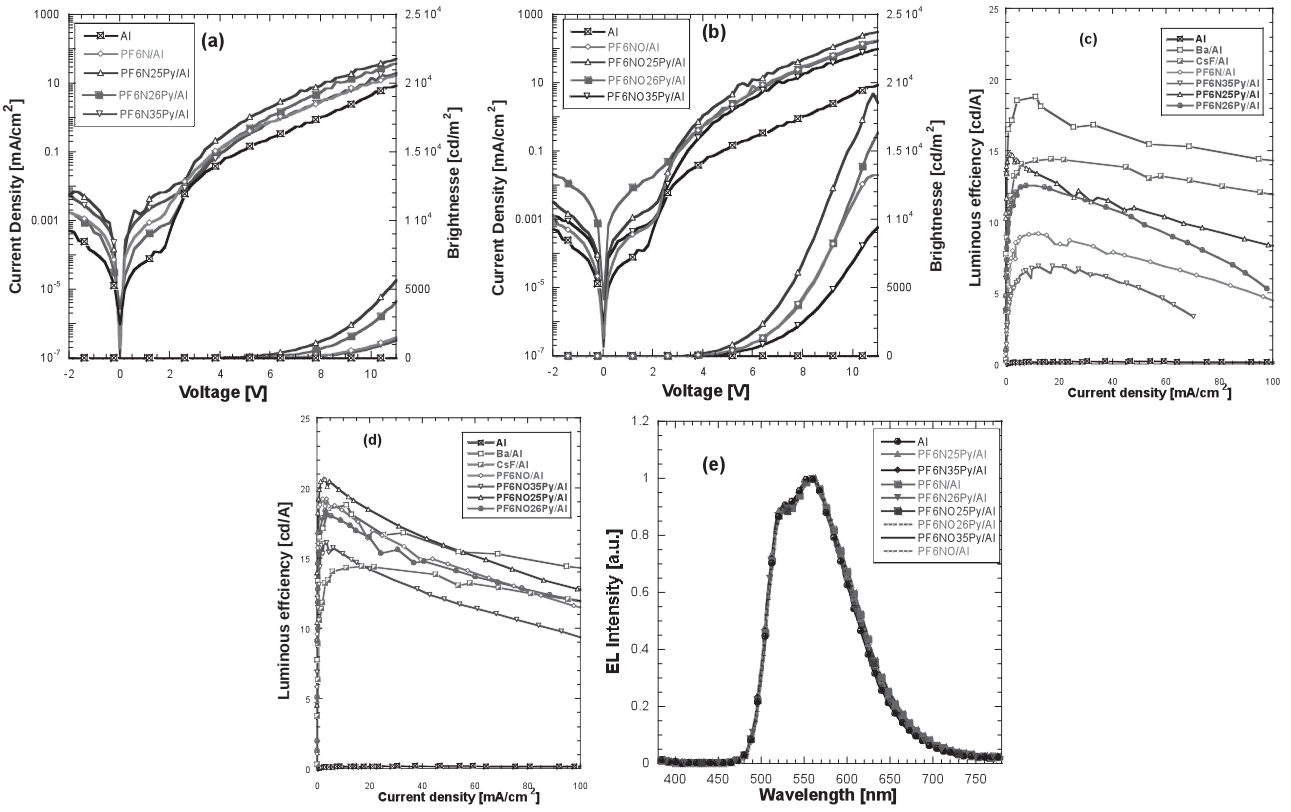

Figure 2. a) *J–L–V* characteristics of PNs/Al cathode devices, b) *J–L–V* characteristics of PNOs/Al cathode devices, c) *LE–J* characteristics of PNs/Al cathode devices, d) *LE–J* characteristics of PNOs/Al cathode devices, and e) EL spectra of the PLEDs. Device configuration: ITO/PEDOT:PSS/P-PPV/cathode.

recombination zones are all in the P-PPV layer. The bare Al cathode device shows poorest device performance with $LE = 0.2$ cd A^{-1} and a luminance of 64 cd m^{-2}. Improvements in *LE* and luminance are observed upon introduction of PF6N, PF6N25Py, PF6N26Py, and PF6N35Py interlayers: $LE = 8.0$, 11.8, 10.8, and 6.3 cd A^{-1} and a luminance = 2809, 4100, 3777, and 2201 cd m^{-2} at $J = 35$ mA cm^{-2}, respectively. The turn-on voltages (V_{on}) decreased from 8.8 V for the bare Al device to 2.8–4.4 V for PN/Al devices, indicating that electron injection from Al was facilitated. This may be attributed to the interfacial dipole between the pendant amino groups and the high work-function metal cathodes, which can lower the injection barrier at the interface.[26]

Devices with PNO/Al cathodes exhibit better performance and lower V_{on} than the PNs/Al devices. PF6NO/Al, PF6NO25Py/Al, PF6NO26Py/Al, and PF6NO35Py/Al showed a *LE* of 15.5, 16.9, 15.3 and 12.9 cd A^{-1} with a luminance of 5008, 5066, 5225, and 4233 cd m^{-2} at $J = 35$ mA cm^{-2}, respectively. The PF6NO25Py/Al cathode device showed the best performance, which is more than ninety times higher than the performance of bare Al cathode device, and outperforms what is observed with CsF/Al (13.2 cd A^{-1}) and Ba/Al (16.3 cd A^{-1}) devices. One plausible reason for the better performance of PF6NO25Py/Al cathode device compared to that of PF6NO/Al cathode device is the incorporation of electron-acceptor pyridinyl unit into polymer main chain could enhance the electron transporting ability of polymers thus improve devices performance.[21] Due to the lesser conjugation length arising from meta-linkages of pyridinyl moieties, PF6NO26Py/Al cathode device showed a slightly lower performance than that of PF6NO25Py/Al cathode device, and PF6NO35Py/Al cathode device showed the lowest performance among these PNOs/Al cathode devices. All of these results clearly show that the PNOs indeed exhibit promising electron injection properties from Al cathode and are excellent candidates as cathode interlayer for PLEDs.

Since PNOs and the corresponding PNs have the same backbones, the reason for the differences in device performance is most reasonably attributed to the surfactant-like side chains. Photovoltaic measurements, shown in **Figure 3**, were carried out to determine the built-in potential across the devices and thereby obtain more insight on the working mechanism of the interlayers.[11b,26] The built-in potential can be estimated from the open circuit voltages (V_{oc}) of the devices, which can be obtained from the *I–V* curve under illumination.[11b] The bare Al cathode device showed a V_{oc} of 1.3 V, while all the PNs and PNOs cathode devices showed higher V_{oc} than that of the bare Al cathode device. It should be noted that V_{oc} decreases from PF6N25Py/Al, PF6N26Py/Al to PF6N35Py/Al, progressively. Similar trends were also observed among PF6NO25Py/Al, PF6NO26Py/Al, and PF6NO35Py/Al cathode devices. These results indicate that polymers with para-linkage of pyridinyl moieties in the backbone have lower barrier height for effective electron injection than polymers with meta-linkages of pyridinyl moieties in the backbone. We also observed that PNOs/Al devices show even higher V_{oc} than that of PNs/Al devices, which indicates that the amino

Table 2. Device performance of PLEDs using different cathodes in device configuration ITO/PEDOT/P-PPV/cathode.

Cathode	V_{on}[a)]	Voltage[b)]	Luminance [cd m^{-2}][b)]	LE [cd A^{-1}][b)]	Maximum Brightness [cd m^{-2}]	Maximum LE [cd A^{-1}]
Al	8.8	13.4	64	0.2	873	0.2
Ba/Al	2.5	4.5	5666	16.3	42 771	18.8
CsF/Al	3.0	6.0	4861	13.2	38 109	14.5
PF6N/Al	4.0	12.4	2809	8.0	4658	9.2
PF6NO/Al	2.6	8.4	4977	15.5	13 284	19.2
PF6N25Py/Al	2.8	10.2	4100	11.8	8633	14.7
PF6NO25Py/Al	2.6	7.4	5010	16.9	19 268	20.7
PF6N26Py/Al	3.4	10.8	3777	10.8	5965	12.6
PF6NO26Py/Al	2.8	8.2	5138	15.3	16 954	18.4
PF6N35Py/Al	4.4	12.2	2201	6.3	2704	6.9
PF6NO35Py/Al	3.0	9.0	4266	12.9	9613	16.1

[a)]The driving voltage at a brightness of 1 cd m^{-2}; [b)]Device performance at a current density of 35 mA cm^{-2}.

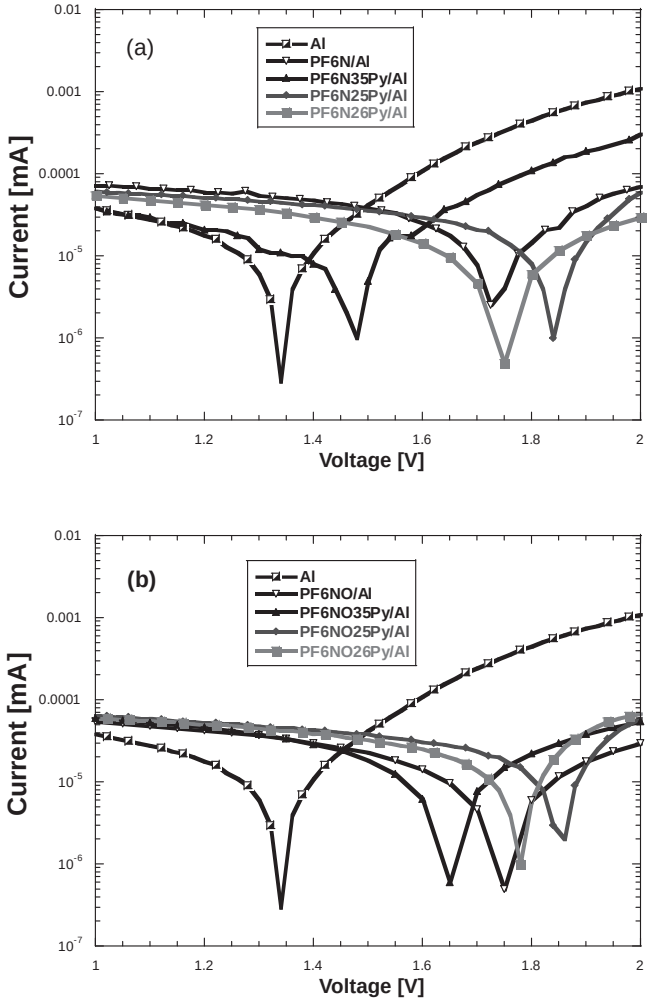

Figure 3. Photovoltaic characteristics of the devices with configuration ITO/PEDOT:PSS/P-PPV/cathode: a) cathode: PNs/Al and b) cathode: PNOs/Al.

N-oxide groups lead to lower energetic barriers for electron. As a result, the PNOs, especially the PF6NO25Py, exhibited a significantly enhanced electron injection properties from Al cathode compared to their precursor polymers PNs, and are excellent candidates as cathode interlayer for PLEDs.

2.4. Cathode Interlayer Function in PSCs

To investigate the electron extraction properties of PNOs in PSCs, a poly[*N*-9′′-hepta-decanyl-2,7-carbazole-alt-5,5-(4′,7′-di-2-thienyl-2′,1′,3′-benzothiadiazole)] (PCDTBT)[27]:[6,6]-phenyl-C_{71}-butyric acid methyl ester ($PC_{71}BM$) blend was used as the active layer in PSCs with device configuration of ITO/PEDOT:PSS/PCDTBT:$PC_{71}BM$/Interlayer/Al. Due to its excellent performance in PLEDs, PF6NO25Py was chosen as the cathode interlayer in PSCs. For comparison, PF6N25Py was also included in these studies.

Figure 4a shows *J*–*V* curves of the devices under 100 mW cm^{-2} air mass 1.5 global (AM 1.5 G) illumination. Figure 4b shows *J*–*V* curves obtained in the dark. **Table 3** summarizes the PSC performance parameters. One finds that PSCs with an Al cathode showed a *PCE* of 4.0%, with a V_{oc} of 0.65 V, a J_{sc} of 11.4 mA cm^{-2}, and a *FF* of 53.8%. This result is consistent with those previously reported studies[12f,12g,27] that PSCs based on PCDTBT:$PC_{71}BM$ with bare Al cathode showed *PCEs* of ≈3 to 5%. Devices with a PF6N25Py/Al cathode showed a significant enhancement in V_{oc}, that could reach 0.90 V, under AM 1.5G illumination, and PF6NO25Py/Al cathode devices showed a even higher V_{oc} of 0.91 V. In dark, devices with a PF6N25Py/Al or PF6NO25Py/Al cathode showed a turn-on voltage of ≈0.9 to 1.0 V, while it was only ≈0.5–0.6 V for the bare Al cathode devices, indicating the V_{bi} across the device significantly increased with the interlayer, thus increased the upper limit of the attainable V_{oc} in PSCs.[28] This phenomenon had also been observed in PLEDs in the above discussion. The significantly enhanced V_{oc} had also been observed in many other WSCPs/Al cathode based PSCs.

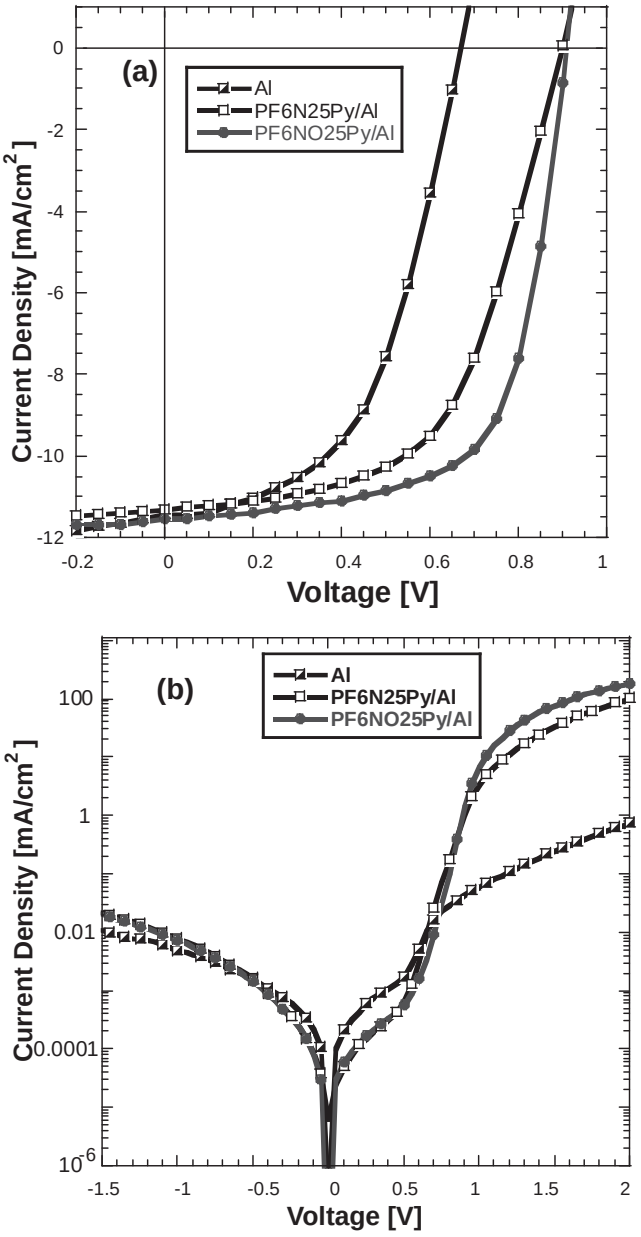

Figure 4. The performance of PSCs with configuration ITO/PEDOT:PSS/PCDTBT:$PC_{71}BM$/cathode. a) *J–V* characteristics of devices under 100 mW cm^{-2} AM 1.5 G illumination and b) *J–V* characteristics of devices in the dark.

Some techniques such as ac impedance spectroscopy[12b] and scanning Kelvin probe microscopy[12f] had been used to explore the WSCPs based devices, and it was found that the interfacial dipole formed by the WSCPs interlayer play an important role on the enhanced V_{oc}. Moreover, devices with the interlayer also showed a higher J_{sc} and *FF*. Especially, PSCs with a PF6NO25Py/Al cathode showed a substantially improved *FF* of 66.2%, which was nearly 20% larger compares to the Al and PF6N25Py/Al devices. PF6NO25Py/Al PSCs also showed the highest J_{sc} (11.6 mA cm^{-2}) among these devices. As a result, high *PCE*s up to 5.7% and 6.9% for the PF6N25Py/Al and PF6NO25Py/Al cathode devices, respectively, have been realized. It has been reported that the *PCEs* of PSCs based on PCDTBT:$PC_{71}BM$ could also reach above 6% by using other cathode interlayers such as TiO_x[29] or bathocuproine.[30] However, the devices using metal oxides typically require a high annealing temperature to achieve a high crystallinity of the metal oxides for good charge carrier mobilities and bathocuproine has to be processed by vacuum deposition. Compared to those previously reported techniques, the solution processible nature of PNOs and PNs make them promising candidates for solution processed polymer solar cells.

Table 3. Performance of PSCs.[a)]

Active Layer	Cathode	J_{sc} [mA cm^{-2}]	V_{oc} [V]	*FF* [%]	*PCE* [%]
PCDTBT:$PC_{71}BM$ (1:4)	Al	11.4	0.65	53.8	4.0
	PF6N25Py/Al	11.3	0.90	56.0	5.7
	PF6NO25Py/Al	11.6	0.91	66.2	6.9

[a)]All the devices were measured under the illumination of AM1.5G at 100 mW cm^{-2}.

3. Conclusions

In summary, a new class of water/alcohol soluble conjugated polymers with neutral, yet highly polar, amino *N*-oxide-functionalized pendant groups and different linkages of pyridinyl moieties in the main chain (PNOs) were designed and synthesized. These PNO materials, together with their amino functionalized precursor polymers (PNs), function as interlayer materials for PLEDs and PSCs. Based on the comparison to PNs, the amino *N*-oxide groups in the PNO structure not only enhance alcohol solubility, but also significantly enhance the ability of interlayers to reduce electron injection barriers. PSCs based on PNOs/Al cathode also exhibit higher V_{oc}, J_{sc}, and *FF* than those of PNs/Al cathode devices. By using PF6NO25Py as cathode interlayer, improvements in performance were achieved that are more than 90 and 1.7 times higher than that obtained with bare Al cathode devices for PLEDs and PSCs, respectively. These results show that PNOs are a new class of materials that can be readily incorporated into device fabrication and lead to desirable improvements in performance.

4. Experimental Section

General Details: All reagents, unless otherwise specified, were obtained from Alfa Aesar or Sigma-Aldrich and used as received. 2,5-dibromopyridine, 3,5-dibromopyridine, and 2,6-dibromopyridine were purified by recrystallization from methanol before use. Some of the solvents used were further purified before use (THF from sodium/benzopheone, acetonitrile from CaH_2, toluene was washed with H_2SO_4 and then treated with $CaCl_2$). ^1H and ^{13}C NMR spectra were measured using a Bruker AV-300. Molecular weights of the polymers were determined by a Waters GPC 2410 in THF using a calibration curve with polystyrene standards. Cyclic voltammetry data were measured on a CHI600D electrochemical workstation by using Bu_4NPF_6 (0.1 M) in acetonitrile as electrolyte and platinum and Ag/Ag+ (0.1 M of $AgNO_3$ in acetonitrile) as the working and reference electrode, respectively. UV-vis

spectra were recorded on a HP 8453 spectrophotometer. PL spectra were recorded on an Instaspec IV CCD spectrophotometer (Oriel Co.). Elemental analyses were performed on a Vario EL elemental analysis instrument (Elementar Co.).

*2,7-Dibromo-9,9-bis(6″(N,N-diethylamino)hexyl)fluorene (**1**)*: To a solution of 2,7-dibromo-9,9-bis(6′-bromohexyl)fluorene (26g, 40 mmol) in DMF (250 mL) under argon, diethylamine (24 mL) was added in one portion. The mixture was refluxed with vigorously stirring overnight under argon atmosphere. After the reaction was cooled to room temperature, the mixture was poured into ice water, and the aqueous layer was extracted with dichloromethane for several times. The organic layer was combined and washed with water and brine, dried over anhydrous magnesium sulphate. After removal of the solvent by rotary evaporation, the residue was purified with column chromatography (silica gel, petroleum/triethylamine) to afford **1** as white solid (21.6g, 85%). ^{1}H NMR (300 MHz, $CDCl_3$, δ): 7.55-7.52 (d, 2H), 7.48-7.47 (d, 4H), 2.51-2.44 (q, 8H), 2.30-2.28 (t, 4H), 1.96-1.90 (t, 4H), 1.30-1.26(m, 4H), 1.09-1.08(m, 8H), 1.07-0.96 (t, 12H), 0.63-0.61 (m, 4H). ^{13}C NMR (300 MHz, $CDCl_3$, δ): 152.45, 139.07, 130.19, 126.13, 121.48, 121.13, 55.64, 52.80, 46.85, 40.14, 29.75, 27.24, 26.74, 23.61, 11.60. Anal. calcd for $C_{33}H_{50}N_2Br_2$: C 62.46, H 7.886, N 4.416; found: C 62.56, H 7.898, N 4.425.

*2,7-Bis(4,4,5,5-tetramethyl-1,3,2-dioxaborolane-2-yl)-9,9-bis(6′-(N,N-diethylamino)hexyl)-fluorene (**2**)*: *N*-butyllithium (30 mL (75 mmol), 2.5 M in hexane) was added dropwise to a solution of **1** (19 g, 30 mmol) in anhydrous THF (250ml) at –78 °C under argon. After stirring for 2 h at –78 °C, 2-isopropoxy-4,4,5,5-tetramethyl-(1,3,2)-dioxaborolane (30.8 mL, 150 mmol) was added in one shot. The reaction mixture was allowed to warm to room temperature and stirred overnight. The mixture was poured into water and extracted with dichloromethane. The combined organic layer was washed with water and brine, dried over anhydrous magnesium sulphate. After removal of the solvent by rotary evaporation, the residue was purified by recrystallization from acetone to afford 2 as colorless crystal (17.9 g, 82%). ^{1}H NMR (300 MHz, $CDCl_3$, δ): 7.81-7,78 (d, 2H), 7.72-7.69 (d, 4H),2.46-2.39 (q, 8H), 2.27-2.22 (t, 4H), 2.01-1.96 (t, 4H), 1.38 (s, 24H), 1.24-1.17(m, 4H),1.01-0.92(m, 20H), 0.54 (m, 4H). ^{13}C NMR(300 MHz, $CDCl_3$, δ): 150.35, 143.89, 133.69,128.86, 119.36, 83.70, 55.11, 52.75, 46.82, 40.14, 29.90, 27.31, 26.66, 24.93, 23.69, 11.54.Anal. calcd for $C_{45}H_{74}B_2N_2O_4$: C 74.18, H 10.16, N 3.846; found: C 74.19, H 10.54, N 3.868.

General Procedure for Preparation Precursor Polymers PNs: Polymerization reactions were carried out by palladium(0)-catalyzed Suzuki cross-coupling reactions. Diboronic ester monomer (0.5 mmol) and dibromo monomer (0.5 mmol) were mixed with $Pd(PPh_3)_4$ (5 mg) in a mixture of 20% aqueous tetraethylammonium hydroxide (1 mL) and toluene (5 mL) under argon. After degassing, the reaction mixture was vigorously stirred at 90 °C for 24 h. After cooling to room temperature, the mixture was poured into methanol. The precipitated material was separated by filtration and washed with acetone for 24 h in a Soxhlet. The obtained solids was dissolved in THF(10 mL), and then filtered with a 0.45 μm polytetrafluoroethylene (PTFE) filter, concentrated, and precipitated from methanol to give the resulting polymers.

PF6N: **1** (0.5 mmol, 317 mg) and **2** (0.5 mmol, 364 mg) were used in the reaction to give PF6N (383 mg, 91%). ^{1}H NMR (300 MHz, $CDCl_3$, δ): 7.82-7.93 (m, 6H), 3.02-3.05 (m, 12H), 2.90-2.93 (m, 4H), 1.98-2.21 (m, 4H), 0.88-1.23 (m, 24H). GPC (THF, polystyrene standard) analysis showed a M_n = 13500 and *PDI* = 1.403.

PF6N25Py: **1** (0.5 mmol, 317 mg) and 2,5-dibromopyridine (0.5 mmol, 118 mg) were used in the reaction to give PF6N25Py (232 mg, 84%). ^{1}H NMR (300 MHz, $CDCl_3$, δ): 9.08 (s, 1H), 7.62-8.15 (m, 8H), 2.40-2.45 (m, 12H), 2.27-2.29 (m, 4H), 1.21-1.24 (m, 4H), 1.08-1.10 (m, 8H), 0.90-0.96 (m, 12H), 0.84 (m, 4H). GPC (THF, polystyrene standard) analysis showed a M_n = 22401 and *PDI* = 1.607.

PF6N26Py: **1** (0.5 mmol, 317 mg) and 2,6-dibromopyridine (0.5 mmol, 118 mg) were used in the reaction to give PF6N26Py (237 mg, 86%). ^{1}H NMR (300 MHz, $CDCl_3$, δ): 8.29-8.31 (m, 2H), 8.16 (s, 2H), 7.81-7.94 (m, 5H), 2.38-2.45 (m, 8H), 2.25-2.30 (m, 4H), 2.18 (m, 4H), 1.25-1.28 (m, 4H), 1.10-1.12 (m, 8H), 0.91-0.97 (m, 12H), 0.81 (m, 4H). GPC (THF, polystyrene standard) analysis showed a M_n = 12100 and *PDI* = 1.587.

PF6N35Py: **1** (0.5 mmol, 317 mg) and 3,5-dibromopyridine (0.5 mmol, 118 mg) were used in the reaction to give PF6N35Py (218 mg, 79%). ^{1}H NMR (300 MHz, $CDCl_3$, δ): 8.90 (s, 2H), 8.23 (s, 1H), 7.91-7.92 (m, 2H), 7.66-7.73 (m, 4H), 2.66-2.73 (m, 8H), 2.50-2.56 (m, 4H), 2.11 (m, 4H), 1.40-1.41 (m, 4H), 1.09-1.11 (m, 8H), 1.02-1.07 (m, 12H), 0.74 (m, 4H). GPC (THF, polystyrene standard) analysis showed a M_n = 10300 and *PDI* = 1.553.

General Procedure for Preparation Polymers PNOs: Hydrogen peroxide (0.5 mL) was added to a mixture of precursor polymers PNs (100 mg) and methanol (10 mL). After vigorously stirring at room temperature for 48 h, the resulting mixture was filtered with a 0.45 μm PTFE filter, concentrated then precipitated from acetic ether, and washed several times with acetic ether and THF to give the resulting polymers.

PF6NO: PF6N was used as precursor polymer in the reaction to give PF6NO (95 mg, 90%). ^{1}H NMR (300 MHz, CD_3OD, δ): 7.82-7.93 (m, 6H), 3.22-3.24 (m, 12H), 3.07-3.18 (m, 4H), 1.56-1.57 (m, 4H), 1.18-1.23 (m, 24H).

PF6NO25Py: PF6N25Py was used as precursor polymer in the reaction to give PF6NO25Py (98 mg, 93%). ^{1}H NMR (300 MHz, CD_3OD, δ): 9.06 (s, 1H), 7.88-8.54 (m, 8H), 3.09-3.12 (m, 12H), 2.87-2.89 (m, 4H), 1.50-1.52 (m, 4H), 0.98-1.18 (m, 24H).

PF6NO26Py: PF6N26Py was used as precursor polymer in the reaction to give PF6NO26Py (94 mg, 89%). ^{1}H NMR (300 MHz, CD_3OD, δ): 8.36-8.53 (m, 4H), 7.98-8.04 (m, 5H), 3.01-3.03 (m, 8H), 2.90-2.91 (m, 4H), 2.31 (m, 4H), 1.46-1.47 (m, 4H), 1.27-1.29 (m, 8H), 1.04-1.09 (m, 12H), 0.86 (m, 4H).

PF6NO35Py: PF6N35Py was used as precursor polymer in the reaction to give PF6NO35Py (88 mg, 84%). ^{1}H NMR (300 MHz, CD_3OD, δ): 8.92 (s, 2H), 8.50 (s, 1H), 8.03-8.05 (m, 2H), 7.88-7.94 (m, 4H), 3.09-3.16 (m, 8H), 2.97-3.01 (m, 4H), 2.30 (m, 4H), 1.53-1.54 (m, 4H), 1.14-1.28 (m, 20H), 0.94 (m, 4H).

Device Fabrication and Characterization: For the PLED devices, a thickness of 40 nm PEDOT:PSS (Baytron P4083, BayerAG) layer was spin-coated on a pre-cleaned ITO substrate and dried by baking at 200 °C for 10 min to remove residual water. Then, 90 nm P-PPV layer was spin-casted onto PEDOT:PSS from p-xylene solution. The electron-injection materials PNs and PNOs were spin-coated onto P-PPV layer from methanol/acetic acid and methanol solution as cathode interlayer, respectively. Finally, a 80 nm thick aluminum was thermally deposited as cathode through a shadow mask (defined active area of 0.19 cm^2) in a chamber with a base pressure of $<5 \times 10^{-4}$ Pa.

For the PSC devices, a thickness of 40 nm PEDOT:PSS (Baytron P4083, BayerAG) layer was spin-coated on a pre-cleaned ITO substrate and dried by baking at 200 °C for 10 min to remove residual water. Then, 80 nm PCDTBT/$PC_{71}BM$ (1/4, w/w) layer was spin-coated onto PEDOT:PSS from 1,2-dichlorobenzene/chlorobenzene (3/1, v/v) solution. The electron-injection materials PNs and PNOs were spin-coated onto active layer from methanol/acetic acid and methanol solution as cathode interlayer, respectively. Finally, a 80 nm thick aluminum was thermally deposited as cathode through a shadow mask (defined active area of 0.16 cm^2) in a chamber with a base pressure of $<5 \times 10^{-4}$ Pa.

The cathode thickness was monitored upon deposition by using a crystal thickness monitor (Sycon). Profilometry (Veeco Dektak150) was used to determine the thickness of the polymer films. Device fabrication was carried out in an N_2 atmosphere dry-box (Vacuum Atmosphere Co.). *J–V–L* data was collected using a Keithley 236 source meter and a calibrated silicon photodiode in the N_2 atmosphere dry-box. After typical encapsulation of the devices with UV epoxy and cover glass, the devices were taken out from dry-box and the external electroluminescence quantum efficiencies (QE_{ext}) were obtained by measuring the total light output in all directions in an integrating sphere (IS-080, Labsphere). *PCE*s were measured under an AM1.5G solar simulator (Oriel model 91192). The power of the sun simulation was calibrated as a value of 100 mW cm^{-2} before the testing using a standard silicon solar cell.

Acknowledgements

The work was financially supported by the Ministry of Science and Technology, China (MOST) National Research Project (No. 2009CB623601 and 2009CB930604) and the Natural Science Foundation of China (No. 21125419, 50990065, 51010003, 51073058 and 20904011). GCB is grateful to the National Science Foundation (DMR-1005546) for financial support.

Received: January 21, 2012
Revised: March 5, 2012
Published online: April 10, 2012

[1] a) J. H. Burroughes, D. D. C. Bradley, A. R. Brown, R. N. Marks, K. Mackay, R. H. Friend, P. L. Burn, A. B. Holmes, *Nature* **1990**, *347*, 539; b) A. C. Grimsdale, K. L. Chan, R. E. Martin, P. G. Jokisz, A. B. Holmes, *Chem. Rev.* **2009**, *109*, 897; c) C. M. Zhong, C. H. Duan, F. Huang, H. B. Wu, Y. Cao, *Chem. Mater.* **2011**, *23*, 326.

[2] a) G. Yu, J. Gao, J. C. Hemmelen, F. Wudl, A. J. Heeger, *Science* **1995**, *270*, 1789; b) C. J. Brabec, *Sol. Energy Mater. Sol. Cells* **2004**, *83*, 273; c) S. Gunes, H. Neugebauer, N. S. Sariciftci, *Chem. Rev.* **2007**, *107*, 1324; d) P. W. M. Blom, V. D. Mihailetchi, L. J. A. Koster, D. E. Markov, *Adv. Mater.* **2007**, *19*, 1551; e) G. Dennler, M. C. Scharber, C. J. Brabec, *Adv. Mater.* **2009**, *21*, 1323; f) C. Li, M. Liu, N. G. Pschirer, M. Baumgarten, K. Müllen, *Chem. Rev.* **2010**, *110*, 6817; g) M. Helgesen, R. Sondergaard, F. C. Krebs, *J. Mater. Chem.* **2010**, *20*, 36; h) F. C. Krebs, T. D. Nielsen, J. Fyenbo, M. Wadstrøm, M. S. Pedersen, *Energy Environ. Sci.* **2010**, *3*, 512.

[3] a) L. M. Chen, Z. Xu, Z. Hong, Y. Yang, *J. Mater. Chem.* **2010**, *20*, 2575; b) H. Ma, H. L. Yip, F. Huang, A. K. Y. Jen, *Adv. Funct. Mater.* **2010**, *20*, 1371.

[4] a) C. Adachi, T. Tsutsui, S. Saito, *Appl. Phys. Lett.* **1990**, *57*, 531; b) D. O'Brien, A. Bleyer, D. G. Lidzey, D. D. C. Bradley, T. Tsutsui, *J. Appl. Phys.* **1997**, *82*, 2662.

[5] a) A. P. Kulkarni, C. J. Tonzola, A. Babel, S. A. Jenekhe, *Chem. Mater.* **2004**, *16*, 4556; b) G. Hughes, M. R. Bryce, *J. Mater. Chem.* **2005**, *15*, 94; c) J. G. C Veinot, T. J. Marks, *Acc. Chem. Res.* **2005**, *38*, 632; d) F. Huang, Y. J. Cheng, Y. Zhang, M. S. Liu, A. K. Y. Jen, *J. Mater. Chem.* **2008**, *18*, 4495; e) R. Stein, F. R. Kogler, C. J. Brabec, *J. Mater. Chem.* **2010**, *20*, 2499; f) F. Huang, H. B. Wu, Y. Cao, *Chem. Soc. Rev.* **2010**, *39*, 2500; g) C. A. Zuniga, S. Barlow, S. R. Marder, *Chem. Mater.* **2011**, *23*, 658.

[6] a) I. D. Parker, Y. Cao, C. Y. Yang, *J. Appl. Phys.* **1999**, *85*, 2441; b) M. Jorgensen, K. Norrman, F. C. Krebs, *Sol. Energy Mater. Sol. Cells* **2008**, *92*, 686.

[7] a) L. S. Hung, C. W. Tang, M. G. Mason, *Appl. Phys. Lett.* **1997**, *70*, 152; b) C. J. Brabec, S. E. Shaheen, C. Winder, N. S. Sariciftci, *Appl. Phys. Lett.* **2002**, *80*, 1288.

[8] a) J. Huang, G. Li, E. Wu, Q. Xu, Y. Yang, *Adv. Mater.* **2006**, *18*, 114; b) G. Li, C.W. Chu, V. Shrotriya, J. Huang, Y. Yang, *Appl. Phys. Lett.* **2006**, *88*, 253503.

[9] K. H. Lee, J. Y. Kim, S. H. Park, S. H. Kim, S. N. Cho, A. J. Heeger, *Adv. Mater.* **2007**, *19*, 2445.

[10] a) Y. Cao, G. Yu, A. J. Heeger, *Adv. Mater.* **1998**, *10*, 917; b) F. L. Zhang, F. Sedar, O. Inganäs, *Adv. Mater.* **2007**, *19*, 1835.

[11] a) F. Huang, H. B. Wu, D. L. Wang, W. Yang, Y. Cao, *Chem. Mater.* **2004**, *16*, 708; b) H. B. Wu, F. Huang, Y. Q. Mo, W. Yang, J. B. Peng, Y. Cao, *Adv. Mater.* **2004**, *16*, 1826; c) X. Gong, S. Wang, D. Moses, G. C. Bazan, A. J. Heeger, *Adv. Mater.* **2005**, *17*, 2053; d) R. Q. Yang, H. B. Wu, Y. Cao, G. C. Bazan, *J. Am. Chem. Soc.* **2006**, *128*, 14422; e) G. Zhou, Y. H. Geng, Y. X. Cheng, Z. Y. Xie, L. X. Wang, X. B. Jing, F. S. Wang, *Appl. Phys. Lett.* **2006**, *89*, 233501; f) S. H. Oh, D. Vak, S. I. Na, T. W. Lee, D. Y. Kim, *Adv. Mater.* **2008**, *20*, 1624; g) C. H. Duan, L. Wang, K. Zhang, X. Guan, F. Huang, *Adv. Mater.* **2011**, *23*, 1665; h) H. H. Lu, Y. S. Ma, N. J. Yang, G. H. Lin, Y. C. Wu, S. A. Chen, *J. Am. Chem. Soc.* **2011**, *133*, 9634; i) S. J. Liu, C. M. Zhong, J. Zhang, C. H. Duan, X. H. Wang, F. Huang, *Sci. Chin. Chem.* **2011**, *54*, 1745; j) C. M. Zhong, S. J. Liu, F. Huang, H. B. Wu, Y. Cao, *Chem. Mater.* **2011**, *23*, 4870.

[12] a) Y. Zhao, Z. Y. Xie, C. J. Qin, Y. Qu, Y. H. Geng, L. X. Wang, *Sol. Energy Mater. Sol. Cells* **2009**, *93*, 604; b) J. Luo, H. B. Wu, C. He, A. Y. Li, W. Yang, Y. Cao, *Appl. Phys. Lett.* **2009**, *95*, 043301; c) S. H. Oh, S. I. Na, J. Jo, B. Lim, D. Vak, D. Y. Kim, *Adv. Funct. Mater.* **2010**, *20*, 1977; d) H. Choi, J. S. Park, E. Jeong, G. H. Kim, B. R. Lee, S. O. Kim, M. H. Song, H. Y. Woo, Jin Young Kim, *Adv. Mater.* **2011**, *23*, 2759; e) Z. C. He, C. Zhang, X. F. Xu, L. J. Zhang, L. Huang, J. W. Chen, H. B. Wu, Y. Cao, *Adv. Mater.* **2011**, *23*, 3086; f) Z. C. He, C. M. Zhong, X. Huang, W. Y. Wong, H. B. Wu, L. W. Chen, S. J. Su, Y. Cao, *Adv. Mater.* **2011**, *23*, 4636; g) J. Seo, A. Gutacker, Y. M. Sun, H. B. Wu, F. Huang, Y. Cao, U. Scherf, A. J. Heeger, G. C. Bazan, *J. Am. Chem. Soc.* **2011**, *133*, 8416.

[13] a) F. Huang, H. B. Wu, J. B. Peng, W. Yang, Y. Cao, *Curr. Org. Chem.* **2007**, *11*, 1207; b) C. V. Hoven, A. Garcia, G. C. Bazan, T. Q. Nguyen, *Adv. Mater.* **2008**, *20*, 3793; c) H. Jiang, P. Taranekar, J. R. Reynolds, K. S. Schanze, *Angew. Chem. Int. Ed.* **2009**, *48*, 4300.

[14] W. J. Zeng, H. B. Wu, C. Zhang, F. Huang, J. B. Peng, W. Yang, Y. Cao, *Adv. Mater.* **2007**, *19*, 810.

[15] a) K. Meerholz, *Nature* **2005**, *437*, 327; b) J. M. Hodgkiss, G. L. Tu, S. A. Seifried, W. T. S. Huck, R. H. Friend, *J. Am. Chem. Soc.* **2009**, *131*, 8913.

[16] C. Hoven, R. Q. Yang, A. Garcia, A. J. Heeger, T. Q. Nguyen, G. C. Bazan, *J. Am. Chem. Soc.* **2007**, *129*, 10976.

[17] a) F. Huang, Y. Zhang, M. S. Liu, A. K. Y. Jen, *Adv. Funct. Mater.* **2009**, *19*, 2457; b) F. Huang, Y.-H. Niu, Y. Zhang, J.-W. Ka, M. S. Liu, A. K.-Y. Jen, *Adv. Mater.* **2007**, *19*, 2010; c) J. F. Fang, B. H. Wallikewitz, F. Gao, G. L. Tu, C. Muller, G. Pace, R. H. Friend, W. T. S. Huck, *J. Am. Chem. Soc.* **2011**, *133*, 683.

[18] S. K. Singh, M. Bajpai, V. K. Tyagi, *J. Oleo. Sci.* **2006**, *55*, 99.

[19] E. P. Linton, *J. Am. Chem. Soc.* **1940**, *62*, 1945.

[20] G. Zhou, G. Qian, L. Ma, Y. X. Cheng, Z. Y. Xie, L. X. Wang, X. B. Jing, F. S. Wang, *Macromolecules* **2005**, *38*, 5416.

[21] S. J. Su, D. Tanaka, Y. J. Li, H. Sasabe, T. Takeda, J. Kido, *Org. Lett.* **2008**, *10*, 941.

[22] a) B. Liu, W. L. Yu, Y. H. Lai, W. Huang, *Chem. Mater.* **2001**, *13*, 1984; b) M. Tammer, L. Horsburgh, A. P. Monkman, W. Brown, H. D. Burrows, *Adv. Funct. Mater.* **2002**, *12*, 447; c) W. Yang, J. Huang, C. Z. Liu, Y. H. Niu, Q. Hou, R. Q. Yang, Y. Cao, *Polymer* **2004**, *45*, 865; d) P. H. Aubert, M. Knipper, L. Groenendaal, L. Lutsen, J. Manca, D. Vanderzande, *Macromolecules* **2004**, *37*, 4087; e) S. P. Liu, S. C. Ng, H. S. O. Chan, *Synth. Met.* **2005**, *149*, 1.

[23] B. Liu, W. L. Yu, Y. H. Lai, W. Huang, *Macromolecules* **2002**, *35*, 4975.

[24] a) H. H. Lu, C. Y. Liu, T. H. Jen, J. L. Liao, H. E. Tseng, C. W. Huang, M. C. Hung, S. A. Chen, *Macromolecules* **2005**, *38*, 10829; b) F. Montilla, R. Mallavia, *Adv. Funct. Mater.* **2007**, *17*, 71.

[25] J. Pommerehne, H. Vestweber, W. Guss, R. F. Mahrt, H. Bassler, M. Porsch, J. Daub, *Adv. Mater.* **1995**, *7*, 551.

[26] H. B. Wu, F. Huang, J. B. Peng, Y. Cao, *Org. Electron.* **2005**, *6*, 118.

[27] N. Blouin, A. Michaud, D. Gendron, S. Wakim, E. Blair, R. N. Plesu, M. Bellette, G. Durocher, Y. Tao, M. Leclerc, *J. Am. Chem. Soc.* **2008**, *130*, 732.

[28] M. C. Scharber, D. Mühlbacher, M. Koppe, P. Denk, C. Waldauf, A. J. Heeger, C. J. Brabec, *Adv. Mater.* **2006**, *18*, 789.

[29] S. H. Park, A. Roy, S. Beaupre, S. Cho, N. Coates, J. S. Moon, D. Moses, M. Leclerc, K. Lee, A. J. Heeger, *Nat. Photonics* **2009**, *3*, 297.

[30] T. Y. Chu, S. Alem, S. W. Tsang, S. C. Tse, S. Wakim, J. P. Lu, G. Dennler, D. Waller, R. Gaudiana, Y. Tao, *Appl. Phys. Lett.* **2011**, *98*, 253301.